Macromolecules

Article

Cite This: Macromolecules 2018, 51, 2872−2886

Physical Networks from Multifunctional Telechelic Star Polymers: A Rheological Study by Experiments and Simulations

Vishal Metri,*[,†,‡] Ameur Louhichi,[§,∥] Jiajun Yan,[⊥] Guilhem P. Baeza,[#] Krzysztof Matyjaszewski,[⊥] Dimitris Vlassopoulos,[§,∥] and Wim J. Briels[†,‡,%]

[†]Computational Chemical Physics, Faculty of Science and Technology, and [‡]MESA+ Institute for Nanotechnology, University of Twente, P.O. Box 217, 7500 AE, Enschede, The Netherlands

[§]Institute of Electronic Structure & Laser, FORTH, P.O. Box 1527, 70013 Heraklion, Crete Greece

[∥]Department of Materials Science & Technology, University of Crete, Voutes Campus, 70013 Heraklion, Crete Greece

[⊥]Department of Chemistry, Carnegie Mellon University, Pittsburgh, Pennsylvania 15213, United States

[#]CNRS, MATEIS, University of Lyon, INSA-Lyon, UMR5510-7 avenue Jean Capelle, F-69621 Villeurbanne, France

[%]ICS 3, Forschungszentrum Jülich, Wilhelm-Johnen-Straße, 52428 Jülich, Germany

Supporting Information

ABSTRACT: The equilibrium mechanical properties of a cross-linked gel of telechelic star polymers are studied by rheology and Brownian dynamics simulations. The Brownian dynamics model consists of cores to which Rouse arms are attached. Forces between the cores are obtained from a potential of mean force model developed by Likos and co-workers. Both experimentally and in the simulations, networks were created by attaching sticker groups to the ends of the arms of the polymers, which were next allowed to form bonds among them in a one to one fashion. Simulations were sped up by solving the Rouse dynamics exactly. Moreover, the Rouse model was extended to allow for different frictions on different beads. In order to describe the rheology of the non-cross-linked polymers, it had to be assumed that bead frictions increase with increasing bead number along the arms. This friction model could be transferred to describe the rheology of the network without any adjustments other than an overall increase of the frictions due to the formation of bonds. The slowing down at intermediate times of the network rheology compared to that of the non-cross-linked polymers is well described by the model. The percentage of stickers involved in forming inter-star bonds in the system was determined to be 25%, both from simulations and from an application of the Green−Tobolsky relation to the experimental plateau value of the shear relaxation modulus. Simulations with increasing cross-link percentages revealed that on approaching the gel transition the shear relaxation modulus develops an algebraic tail, which gets frozen at a percentage of maximum cross-linking of about 11%.

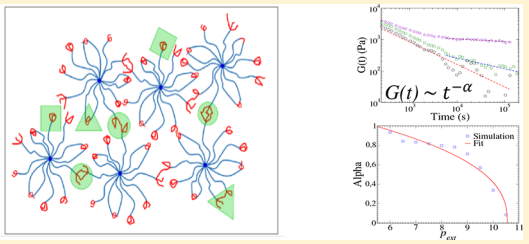

1. INTRODUCTION

Supramolecular polymeric structures are characterized by reversible bond formation which reflects the action of noncovalent bonds such as hydrogen, ionic, or metal−ligand bonds.[1−6] The interplay of association lifetime with the polymeric time scale dictates the strength and stability of the formed assemblies.[7] The former depends on the fraction, functionality, and localization of the bonds, and the latter on the size of polymer segments (between bonds), which may exhibit Rouse-like and disentanglement relaxation. As a result, associating polymeric networks possess intriguing tunable properties such as enhanced elasticity, shape memory, and self-healing.[8−19] Whereas the dynamics of nonionic polymers of different molecular weights and architectures is reasonably well-understood,[20−23] the situation with associating polymers is more complicated. Clearly, the dynamics of supramolecular networks is highly dependent on bond formation and destruction, polymer dynamics, and the properties of segments between bonds.[24,25] Starting from the network plateau accounted for by the Green−Tobolsky model,[26] the dynamics of associating polymers containing reversible bonds can be described through the breaking and reformation process coupled to chain relaxation by means of the sticky-Rouse[27] or sticky reptation[28] models. The former predicts that with decreasing frequency a transition takes place in the storage modulus G' from Rouse dynamics ($G' \propto \omega^{0.5}$) toward a plateau that reflects the number density of elastically active strands. Eventually, the terminal regime ($G' \propto \omega^2$) is reached when the sticky groups dissociate. The latter model is similar in nature and predicts that reptation of the chain along its tube is not possible before the stickers disassociate. Briefly, at times longer than the Rouse time of a strand localized between two entanglements and/or stickers τ_e, but shorter than the sticker dissociation time τ, a first plateau modulus (G_1) appears, similar

Received: December 8, 2017
Revised: March 26, 2018
Published: April 3, 2018

DOI: 10.1021/acs.macromol.7b02613
Macromolecules 2018, 51, 2872−2886

to that observed in permanently cross-linked networks. It includes two contributions, from associations and entanglements: $G_1 = \rho RT(1/M_x + 1/M_e)$, where M_x is the mass between two stickers and M_e is the mass of an entanglement strand. At time $t > \tau$, the stress due to the stickers relaxes, and the modulus drops to the entanglement level $G_2 = \rho RT/M_e$. The second plateau persists until the terminal relaxation time of the reversible network, $\tau_{terminal}$, which is longer than the terminal relaxation time of the respective entangled system without associations. Note that the strength of the physical bonds dictates the dynamics. If they are very strong (as in the present case), the sticker relaxation time τ is prohibitively long to allow for an experimentally accessible terminal relaxation of the network. Hence, the network is not reversible during experimental times, albeit physical.

The above framework, irrespective of the strength of physical bonds, has proven to be highly successful and opened the route for designing and engineering topologically complex macromolecules with selective functionalization, which allows tailoring properties in order to meet specific technological needs and at the same time understanding complex processes occurring in nature.[29−31] Therefore, several outstanding challenges should be addressed in this context. One prominent example is developing quantitative predictions for the coupling of supramolecular interactions and topological effects in polymeric systems with branching architectures.[32−35] Given this background, coupling highly branched architectures with multifunctional associating groups is expected to yield novel features due to their ability to link more than two chains at a time and their capacity to form stronger assemblies, while making the system dynamics and the associated physics richer, albeit more complex. The various possibilities for junctions formation in an associated physical network in such situations are illustrated in Figure 1. The finger-like configuration for the

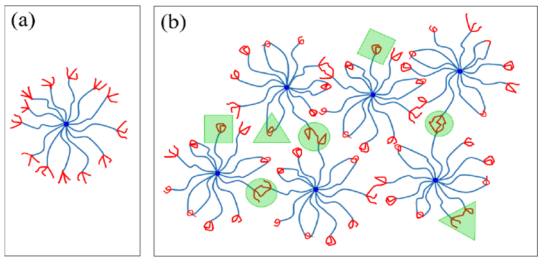

Figure 1. Schematic of the un-cross-linked precursor (a) and the cross-linked network (b). Circles show bonds between stars (inter-star), triangles show bonds between two different arms of the same star (intra-star), and squares show the finger-like stickers closing up among themselves to form an intra-arm bond.

multifunctional associating groups (Figure 1a) is responsible for linking two or more different stars through one or more associations (inter-star) (circles in Figure 1b), often with very high activation energy. Concomitantly, two or more arms from the same star can associate (intra-star) (triangles in Figure 1b) or simply the fingers of the same arm can bridge (intra-arm) (squares in Figure 1b). These different possibilities may facilitate the reformation of junctions after breakup (temperature or shear-induced) through an inter-star/intra-star dynamic exchange, which could also promote the self-healing ability of the network.[18] It should be remarked that self-healing can be expected to be more effective in the case of very strong associations. Related aspects of the sulfur−sulfur bond are addressed in the recent literature.[18,36−38]

As described above, recent developments in polymer chemistry have enabled the synthesis of well-defined star polymers with multifunctional associating groups, which can serve as models for testing these ideas and their consequences on network dynamics.[18,39] On the other hand, for the latter, and more generally, a deeper understanding of the macroscopic response of these systems in relation to their internal microstructure, it is often needed to resort to simulations.[16] However, before assessing the self-healing properties, it is important to rationalize and control the rheology of this class of telechelic stars. This can be achieved with a combination of well-controlled synthesis, rheological experiments, and Brownian dynamics (BD) simulations, which represent the thrust of the present work.

The star polymers investigated here consist of a cross-linked ethylene glycol diacrylate (EGDA) core with an average of 13 arms made of poly(*n*-butyl acrylate) attached to it and with three bis(2-methacryloyloxyethyl) disulfide (DSDMA) stickers (fingers) at the tip of each arm. Stickers can bind strongly to those from other arms and thereby form a cross-linked physical network (see Figure 1). The system is coded as SS3 (disulfide cross-linked with three stickers at the arm tip). The linear viscoelastic response is measured by means of dynamic oscillatory measurements using appropriate protocols to ensure proper equilibration and applying the principle of time−temperature superposition (TTS). Simulation studies of cross-linked networks have been reported before.[16,40−43] In this study we concentrate on the rheological behavior of this strong physical network, starting from its un-cross-linked precursor, which has no stickers at the arm ends and build up a cross-linked network from this system. The stress relaxation modulus $G(t)$ of the cross-linked network decays much slower than that of its precursor and with increasing cross-link percentage develops a terminal plateau characteristic of gelation. This poses severe problems for BD simulations as the speed of the simulation is set by the time scale of the early decay. Since, however, the arm lengths in our system are smaller than an entanglement length and the system is in a melt state, the standard Rouse model may be assumed to describe the dynamics of the arms and strands between connected cores.[44,45] This allows us to simulate the latter analytically without any restriction on the time step by sampling from a Gaussian distribution.[46−48] As a result, the time step is now limited by the diffusion of the cores which is much slower than the early decay of the shear relaxation modulus. In addition to this, we present a generalized version of the Rouse model by proving that the Rouse modes of a polymer are uncorrelated, even when an arbitrary distribution of frictions of the beads is being used. Extensions of the Rouse model to incorporate more than one friction have been suggested before. However, these studies were restricted to systems with just two different friction coefficients[49−51] or used a random distribution of frictions to incorporate dynamic asymmetry.[52−54] Here we provide a completely general method, allowing us to sample from a Gaussian distribution even in cases where all the beads have different frictions. In order to establish model parameters associated with the dynamics, we first study the linear rheology of the precursor by both simulations and experiments.

The remainder of this paper is arranged as follows. We first present the simulation models used to describe the precursor and the network. Next, we present the experimental system, its

DOI: 10.1021/acs.macromol.7b02613
Macromolecules 2018, 51, 2872−2886

synthesis and molecular characterization, and give some additional details of the experimental and simulation methods used. We then continue with presenting the results and analysis from the comparison of simulation and experimental data. Finally we summarize the key conclusions and perspectives.

2. SIMULATION MODEL

In this section we first describe the model that we have used to simulate the rheology of the precursor, a system containing star polymers with functionality f and without connections between the arms on different stars. In the last subsection, we indicate what changes we made to simulate the cross-linked systems in which some arms are allowed to connect through interactions at telechelic ends and by this form bridges from one star to another.

2.1. Model Hamiltonian and Propagator. *2.1.1. Precursor.* The most detailed picture of a star-polymer system, relevant for rheology, is the one in which the positions and interactions of all segments are considered as a function of time. At a somewhat coarser level, one might consider all positions and interactions of groups of segments having the size of a Kuhn length. Using a model like this, in principle, would allow the calculation of configurational properties such as, for example, the distribution of the cores in the case of star polymers and also of rheological properties from time scales of a few tenths of nanoseconds all the way to minutes. Unfortunately, with a model like this it would be impossible to reach the large time scales of interest in the present paper by means of computer simulations. We therefore suggest an even coarser model, thereby obviously losing some accuracy with our predictions.

The Hamiltonian of our model is given by

$$H_{\text{precursor}} = \sum_{I=1}^{N_t-1} \sum_{J=I+1}^{N_t} \phi(r_{IJ}) + \sum_{I=1}^{N_t} \phi^I_{\text{Rouse}} \tag{1}$$

The sum over pairs represents entropic interactions between two stars I and J, with $r_{IJ} = |\vec{r}_I - \vec{r}_J|$ being the distance between their cores and with $\vec{r}_I$ being the position of the core of the Ith star. N_t is the total number of stars in the system. The pair contributions $\phi(r_{IJ})$ are given by the so-called Likos potential:[55]

$$\phi(r_{IJ}) = \left(\frac{5k_BT}{18}\right) f^{1.5} \left[-\ln\left(\frac{r_{IJ}}{\sigma}\right) + \left(1 + \frac{\sqrt{f}}{2}\right)^{-1} \right] \qquad r_{IJ} \le \sigma$$

$$= \left(\frac{5k_BT}{18}\right) f^{1.5} \left(1 + \frac{\sqrt{f}}{2}\right)^{-1} \left(\frac{\sigma}{r_{IJ}}\right) \exp\left(-\sqrt{f}\left(\frac{r_{IJ} - \sigma}{2\sigma}\right)\right) \qquad r_{IJ} > \sigma \tag{2}$$

where f is the number of arms of the star. The first line in eq 2 describes repulsions at distances smaller than σ, while the second line describes the smooth decay of these repulsions to zero at larger distances.

Let us briefly discuss the status of the Likos potential. As mentioned above, ideally we would study the dynamics of all Kuhn segments in the system as governed by the mutual interactions applicable at that level. Having done a simulation like this, one might be interested in the distribution of the cores. In order to find this distribution, P, and the corresponding potential, $-k_BT \ln P$, one would simply average over, i.e. "integrate out", all other degrees of freedom. One would end up with the exact distribution and the exact potential. This potential also governs the exact average forces between cores and is therefore called the potential of mean force. The Likos potential is a pairwise approximation of this potential.[55] It is the best potential available today to describe the configurations and dynamics of the cores of stars.

Figure 2 shows the Likos potential for stars with 13 arms and for comparison also for stars with 40 arms. With increasing

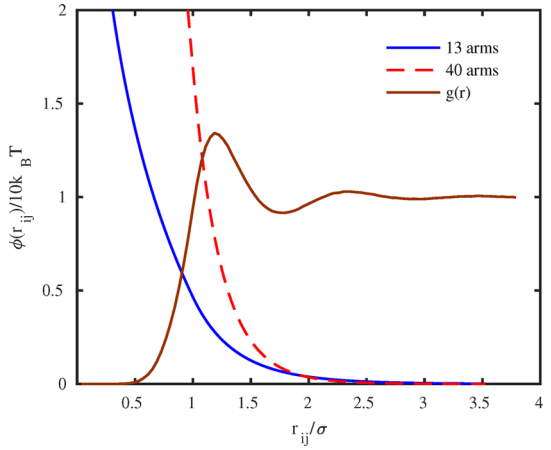

Figure 2. Potential of mean force as a function of dimensionless inter-star distance for two stars with functionality equal to 13 and 40. The brown line represents the resulting radial distribution function $g(r)$ for a melt of 13-arm stars.The parameter σ is fixed by setting the pressure equal to one atm for the given number density.

functionality, star polymers become increasingly colloid-like in nature,[56] which can be seen by the potential becoming steeper when f increases from 13 to 40. The radial distribution function, simulated with a melt of 13 arm stars interacting via the Likos potential, is also drawn in that figure and clearly shows how the excluded volume prevents the stars from approaching each other to small distances. We will discuss this picture below.

In order to be able at a later stage to study networks, we need the positions of the stickers. We obtain them by adding chains to the cores, 13 to each core since this corresponds to the actual experimental system. In order not to influence the distribution of the cores, we choose to add Rouse arms, also called "phantom arms", whose dynamics is governed by the second term in eq 1, with

$$\phi^I_{\text{Rouse}} = \frac{1}{2} k_s \sum_{a=1}^{f} \sum_{n=1}^{N} |\vec{R}^I_{a,n} - \vec{R}^I_{a,n-1}|^2 \tag{3}$$

which is nothing but the sum of the free energies stored in the entropic springs connecting consecutive beads along the f arms of the Ith star. $\vec{R}^I_{a,n}$ denotes the position vector of the nth bead along the ath arm of the Ith star, and N is the number of Kuhn segments (beads) on each arm, 7 in the case of our precursor. The first bead of each arm a is connected to the central core with position vector $\vec{r}_I = \vec{R}^I_{a,0}$. The spring constant is

$$k_s = \frac{3k_BT}{b^2} \tag{4}$$

where b is the Kuhn length. The arms are called "phantom arms" because no contributions to the potential energy prevent the arms from crossing each other. It is well-known that with relatively short arms the Rouse model mimics the motion of the Kuhn segments quite well. A somewhat better model might be based on FENE springs rather than the harmonic springs of the Rouse model, but this would not allow for the speed up of the

DOI: 10.1021/acs.macromol.7b02613
Macromolecules 2018, 51, 2872−2886

arm dynamics that we describe below. Besides providing the positions of the stickers, the Rouse arms also reinstate fast stress fluctuations, which had been removed by the procedure to calculate the Likos potential, thereby allowing the calculation of rheological properties at shorter time scales.

During a time step dt, each bead or core, with position vector $\vec{R}^I_{a,n}$, is displaced according to

$$\mathrm{d}\vec{R}^{\,I}_{a,n}(t) = -\frac{1}{\xi_n}\frac{\partial H}{\partial \vec{R}^{\,I}_{a,n}}\,\mathrm{d}t + \vec{F}^I_{a,n}\,\mathrm{d}t \tag{5}$$

where ξ_n is a friction coefficient and $\vec{F}^I_{a,n}$ equals $\sqrt{\frac{2k_BT}{\xi_n\,\mathrm{d}t}}\,\vec{\Theta}^{\,I}_{a,n}$ with $\vec{\Theta}^I_{a,n}$ being a zero mean, unit variance Gaussian vector. Notice that we allow for the possibility that different beads have different friction coefficients, the distribution of these frictions being the same on each arm and each polymer.

2.1.2. Network. In the absence of any interactions between the beads in the arms on different stars, the only way their motions can be correlated is through the movements of the cores. In general, the frictions on the cores will be much larger than those on the other beads. Therefore, the displacements of the cores due to interactions with surrounding stars will be very small on time scales that are characteristic for the Rouse dynamics. In that case the internal dynamics of the individual stars and their contributions to rheological properties of interest can be solved analytically, and there is no need to include the Rouse part of the Hamiltonian in a full simulation of the system. This is not true once we have connected a fraction of the arms in order to form a network. In this case, however, we must deal with the fact that the small friction on the beads asks for time steps which are very small to sample all relevant configurations of the cores. In the next subsection we describe how the dynamics of the Rouse part of the Hamiltonian can be simulated efficiently using large time steps and later indicate changes to be made after bridges have been formed.

The main objective of our investigations is to simulate the stress response of the networks obtained by cross-linking some of the ends of the stars to form bridges from one core to another. In particular, we are interested in how the shear relaxation moduli of such systems change with varying cross-link percentages. The network forming star is exactly the same as the precursor except for the presence of an eighth bead representing a sticker group at the end of each arm. After the creation of a network we have, in addition to dangling arms, loops from one core back to itself and bridges from one core to another. In the first case we simply ignore the additional sticker group, while in the other two cases we combine the two sticker groups forming the bond into one bead, leaving us with $2N + 1$ beads of which bead number $N + 1$ represents the two stickers. With these assumptions, the Hamiltonian is given by

$$H_{\mathrm{network}} = \sum_{I=1}^{N_t-1}\sum_{J=I+1}^{N_t}\phi(r_{IJ}) + \sum_{I=1}^{N_t}\phi^I_{\mathrm{UNCON}} + \sum_{I=1}^{N_t-1}\sum_{J=I+1}^{N_t}\phi^{IJ}_{\mathrm{CONN}} \tag{6}$$

with

$$\phi^I_{\mathrm{UNCON}} = \frac{1}{2}k_s\sum_{a=1}^{f^I_{\mathrm{UNCON}}}\sum_{n=1}^{N_s}|\vec{R}^{\,I}_{a,n} - \vec{R}^{\,I}_{a,n-1}|^2 \tag{7}$$

$$\phi^{IJ}_{\mathrm{CONN}} = \frac{1}{2}k_s\sum_{a\in C(I,J)}\sum_{n=1}^{2N+2}|\vec{R}^{\,IJ}_{a,n} - \vec{R}^{\,IJ}_{a,n-1}|^2 \tag{8}$$

Here, $\phi(r_{IJ})$ is the same potential of mean force (Likos potential) as in the case of the precursor. ϕ^I_{UNCON} is the Rouse potential given in eq 3, where f^I_{UNCON} is the number of arms of star I that are not connected to any other star; in the case of dangling arms $N_s = N$ and in the case of loops $N_s = 2N + 2$, with bead number $N + 1$ representing the two merged stickers as mentioned before. As before $\vec{R}^I_{a,0} = \vec{r}_I$, while also $\vec{R}^I_{a,2N+2} = \vec{r}_I$ in this case. In the second line, $\phi^{IJ}_{\mathrm{CONN}}$ is the Rouse potential for connected arms between stars I and J, where $C(I,J)$ is the set of arms connecting these stars; in this case, the first N beads in the bridges represent the ones contributed by star I with $\vec{R}^{IJ}_{a,0} = \vec{r}_I$, bead number $N + 1$ represents the two merged stickers, and beads $N + 2$ up to $2N + 1$ represent the beads contributed by star J with $\vec{R}^{IJ}_{a,2N+2} = \vec{r}_J$. In case $C(I,J)$ is empty, the pair IJ does not contribute to $\phi^{IJ}_{\mathrm{CONN}}$.

Notice that we have left the contribution of the core−core potential of mean force unchanged, still being described by the same Likos potential as we used for the precursor.

2.2. Normal Mode Simulation Method with Nonuniform Friction Coefficients. Explicit solutions of the dynamics of many Rouse systems have been published in the literature.[44−48] The reason that so many individual cases have been treated is that the authors were interested in full analytical solutions that could be explicitly written down. Here, we are satisfied with any procedure that allows for a very quick solution, possibly involving some computationally efficient numerical calculations. Moreover, we want to be able to treat systems in which the friction forces may differ among the various beads in the system. Since solutions of the Rouse dynamics of such general systems does not seem to be easily accessible in the literature, we briefly outline how to update the configuration of Rouse systems with time steps dt of any value. For simplicity, we discriminate the various beads by just a single index, writing for the position vectors of the beads $\vec{R}_i$. With this notation the equations of motion read

$$\frac{\mathrm{d}\vec{R}_i}{\mathrm{d}t} = -\frac{w}{m_i}\sum_j T_{ij}\vec{R}_j + \frac{\vec{F}_i}{\sqrt{m_i}} \tag{9}$$

Here $w = k_s/\xi_0$ is the so-called Rouse rate with ξ_0 being some reference friction, and $m_i = \xi_i/\xi_0$. The factor of $1/\sqrt{m_i}$ in the last term has been introduced for notational convenience. The vector $\vec{F}_i$ then represents random displacements resulting from small scale dynamics eliminated from the description. As before, it is assumed to be a Gaussian random vector with uncorrelated random components given by $\sqrt{\frac{2k_BT}{\xi_0\,\mathrm{d}t}}\,\vec{\Theta}_i$ with $\vec{\Theta}_i$ being a zero mean unit variance random vector. The Rouse matrix $\mathbf{T}$ with elements T_{ij} is the incidence matrix of the system describing which pairs of beads are connected to each other through springs with spring constant k_s. By its very definition the Rouse matrix is symmetric. An example of a Rouse matrix for star polymers is given in Liu et al.[57] and Zimm and Kilb.[58]

A set of linear equations like eq 9 is most easily solved by diagonalizing the corresponding interaction matrix. In order that the resulting modes, called Rouse modes in the present case, are independent, the stochastic contributions to the Rouse mode dynamics must be uncorrelated. This will automatically be ensured if the transformation matrix that diagonalizes the

DOI: 10.1021/acs.macromol.7b02613
Macromolecules 2018, 51, 2872−2886

interaction matrix is orthogonal, which fact is not apparent when the frictions are all different as the factors m_i in the denominators complicate the procedure. Therefore, we first symmetrize the interaction matrix by introducing coordinates $\vec{Q}_i$ according to $\vec{Q}_i = \sqrt{m_i}\vec{R}_i$. The equation of motion then reads

$$\frac{d\vec{Q}_i}{dt} = -w\sum_j T^m_{ij}\vec{Q}_j + \vec{F}_i \tag{10}$$

with $T^m_{ij} = T_{ij}/(\sqrt{m_i m_j})$, which is still symmetric and therefore has an orthogonal diagonalizing matrix. Note that this procedure also works when the springs are all different. In this case, the differing spring constants must be moved into the Rouse matrix **T**, which, however, still is symmetric.

We now proceed in the usual way, defining

$$\vec{X}_k = \sum_{i=1}^{N}\vec{Q}_i S_{ik} \tag{11}$$

with $\mathbf{S} = (S_{ik})$ being the orthogonal matrix that diagonalizes the Rouse matrix, i.e., $\mathbf{S}^T\mathbf{T}^m\mathbf{S} = \mathbf{\Lambda}$. An important point is that **S** can be calculated once and for all at the start of the simulation. Equation 11 can easily be inverted to obtain $\vec{Q}_i = \sum_{k=1}^{N} S_{ik}\vec{X}_k$, so one can switch between using Rouse mode vectors $\vec{X}_k$ and bead position vectors $\vec{R}_i = \sqrt{m_i}\vec{Q}_i$. The Rouse mode vectors at any time may now be obtained according to

$$\vec{X}_k(t) = \vec{X}_k(0)e^{-t/\tau_k} + \int_0^t e^{-(t-t')/\tau_k}\vec{G}_k(t')\,dt' \tag{12}$$

$$\vec{G}_k(t) = \sum_{i=1}^{N}\vec{F}^m_i(t)S_{ik} \tag{13}$$

Here $\tau_k = \frac{1}{\omega\lambda_k} = \frac{\xi_0}{k_s\lambda_k}$ is the characteristic time of mode k, while λ_k is the k'th eigenvalue in matrix $\mathbf{\Lambda}$ defined above. $\vec{G}_k(t)$ is a sum of Gaussian vectors, and therefore is itself a Gaussian vector. Similarly, the integral in eq 12 is a Gaussian vector with mean zero and variance $\sigma_k(t)^2$, which can easily be obtained from the properties of $\vec{F}^m$. The updates for the Rouse vector $\vec{X}_k$ then becomes

$$\vec{X}_k(t + dt) = \vec{X}_k(t)e^{-dt/\tau_k} + \sigma_k(dt)\vec{\Theta}_k \tag{14}$$

$$\sigma_k(dt) = \sqrt{\frac{k_B T}{\xi_0}\tau_k(1 - e^{-2dt/\tau_k})} \tag{15}$$

These equations solve the Rouse dynamics exactly, so dt may take any value. Our time step is now not limited anymore by the fast dynamics of the Rouse system and may therefore be adjusted to the dynamics of the cores. Once the eigenvalues of the Rouse matrix are known, the contribution of the Rouse dynamics to the shear relaxation modulus may easily be calculated (see eq 20).

We verified our code by comparing simulation and theoretical results for various time steps and friction models. Moreover, we verified that the radial distribution function of the cores is not influenced by the introduction of the arms.

2.3. Arms and Bridges. As mentioned before, because of the slowness of the motion of the cores, the internal Rouse dynamics of the individual stars may be calculated independently of the motion of the cores during time step dt set by the core dynamics. Assuming, as we do, that the friction on the cores is much larger than that on the other beads, one may expect that a star may be considered as consisting of a fixed core with f arms attached to it. This is corroborated by the following observations concerning the spectrum of the internal modes. Besides the diffusive mode with eigenvalue equal to zero, there are Nf internal modes. N of these give rise to a unique spectrum while the remaining ones give rise to $f - 1$ degenerate spectra, each consisting of N eigenvalues. So, in total there are $N + (f - 1)N = fN$ internal modes and one translational mode. The degenerate spectra are each exactly equal to the spectrum of one arm attached to a fixed core. With increasing values of the core friction, the eigenvalues of the unique spectrum gradually change in order to finally become equal to those of the degenerate spectrum which remained unchanged all the time.

We conclude that the spectrum of a star with high enough functionality consists of f degenerate spectra, all equal to that of one arm with N beads attached to a fixed core (see Figure 3a).

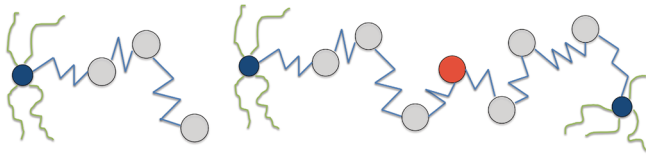

Figure 3. (a) Schematic drawing of an arm modeled as a Rouse chain attached to a core at one end; only three beads are shown for clarity. (b) Picture of two arms bridging two cores. Each of the two arms has been provided with a sticker group at its end, which subsequently have formed a short-range bond resulting in one additional red bead representing the merged mass of the two sticker groups.

Since $G(t)$ is only dependent on the eigenvalues and not on the eigenvectors, we may replace the full Rouse dynamics with that of stars consisting of fixed cores with f independent arms attached to them. The precise way to handle this case is given further down in this subsection.

We now describe the propagator for networks. In the case of bridges and loops, the equation of motion reads

$$\frac{d\vec{Q}_n}{dt} = -w\sum_m T^m_{nm}\vec{Q}_m + \frac{w}{\sqrt{m_n}}(\delta_{n,1}\vec{r}_I + \delta_{n,2N+1}\vec{r}_J) + \vec{F}_n \tag{16}$$

where $\delta_{n,N}$ is the Kronecker delta, being zero except if $n = N$, in which case it equals one. The additional terms are due to the connection of beads number one and $2N + 1$ to cores I and J, respectively. The Rouse matrix **T** with elements $T_{mn} = \sqrt{m_m m_n}\,T^m_{mn}$ is shown below and has size of 15 × 15. The analytical solution of the Rouse modes now becomes

$$\vec{X}_k(t) = \vec{X}_k(0)e^{-t/\tau_k} + \left(\frac{S_{1,k}}{\sqrt{m_1}}\vec{r}_I + \frac{S_{2N+1,k}}{\sqrt{m_{2N+1}}}\vec{r}_J\right)\frac{1}{\lambda_k} \times (1 - e^{-t/\tau_k}) + \int_0^t e^{-(t-t')/\tau_k}\vec{G}_k(t')\,dt' \tag{17}$$

In the second case, i.e., when the $(2N + 1)$ long chain is looping from core I back to core I, one just has to put $\vec{r}_J = \vec{r}_I$. In the case of a dangling arm attached to core I, one simply puts $\vec{r}_J = \vec{0}$ and replaces the Rouse matrix by the one given, whose size now is 7 × 7.

DOI: 10.1021/acs.macromol.7b02613
Macromolecules 2018, 51, 2872−2886

$$\mathbf{T}_{7\times7} = \begin{bmatrix} 2 & -1 & 0 & \cdots & 0 \\ -1 & 2 & -1 & \cdots & 0 \\ \vdots & \vdots & \vdots & \vdots & \vdots \\ 0 & \cdots & -1 & 2 & -1 \\ 0 & \cdots & 0 & -1 & 1 \end{bmatrix}$$

$$\mathbf{T}_{15\times15} = \begin{bmatrix} 2 & -1 & 0 & \cdots & 0 \\ -1 & 2 & -1 & \cdots & 0 \\ \vdots & \vdots & \vdots & \vdots & \vdots \\ 0 & \cdots & -1 & 2 & -1 \\ 0 & \cdots & 0 & -1 & 2 \end{bmatrix}$$

The stochastic term in eq 17 is obtained as before.

We finally summarize the sequence of updates during a time step in the case of networks. First, all cores are moved according to Brownian dynamics with forces derived from the Likos potential. Next, all beads in dangling arms are updated according to the equations also used in the case of the precursor. Finally, all loops and bridges are updated according to the methods of the present section.

It is worth mentioning one consequence of the use of phantom arms that will not be shared by the real system. Creating cross-links in an experimental system will most probably severely slow down the dynamics of the cores. This will also hold true for any simulation model in which the beads experience mutual repulsive interactions besides the spring interactions present in the Rouse model or in which other means have been introduced to avoid crossings of chains.[59,60] In the present model this can only be achieved by adjusting the frictions on the beads and the cores. Besides this, the finite extensibility of the bridges between the cores will limit the volume that the cores can explore. This is not the case with our phantom bridges, since the Gaussian springs between the beads can in principle be stretched beyond any limit, although with increasingly lower probability. This can be prevented by using finitely extensible bonds, but then the possibility to use large time steps as described above will be lost.

3. MATERIALS AND METHODS

3.1. Synthesis and Characterization. The synthesis of the precursor and the gel are described by Kamada et al.[39] In this reference, the authors synthesized and measured the sizes of stars consisting of ca. 23 arms containing ca. 63 PnBA units each, attached to a cross-linked EGDA core.

The present system was synthesized according to the same procedure, except that as initiator we used methyl 2-bromopropionate instead of ethyl 2-bromopropionate. The first step consists of synthesizing an EGDA microgel, whose molecular mass was estimated to be about 6600 g/mol, leading to a diameter of about 1.4 nm. This is the "chemical core" to which the arms are attached in the second step. Using light scattering experiments, the average molecular mass of the stars was measured. We estimated that on average each star contained 13 arms of mass 16 662 g/mol each, equivalent to ca. 130 PnBA units. This is the system that we refer to as the precursor. It is important to realize that the "chemical core" referred to here is not the "core" that we mentioned when describing the model (section 2.1.1). The latter will be further discussed below in relation to the rheology of the precursor and shown to have a diameter of about 6 nm (section 4.1)

Next, the system was cross-linked to form a *gel* by adding sticker groups of DSDMA, to the end of each arm, and allowing the stickers to equilibrate. In principle, each arm was provided with one group of three stickers. As a result of simultaneous growth and gelation of the system, the distribution of the stickers over the arms may not be very sharp; there may be arms with more than three stickers and arms with no stickers. More details are presented in the Supporting Information.

3.2. Molecular and Simulation Parameters. In order to determine parameters in Hamiltonian eq 1, we have proceeded as follows. First, the functionality f was put equal to its average value of 13. For the precursor, this is a harmless assumption, since the Rouse dynamics of a star is to a very good approximation equal to that of f individual arms attached to a fixed point. Besides this, we also removed any polydispersity of the length of the arms. We will argue in section 4.1 that the dynamics of the precursor will be influenced by this assumption only to a small degree, not affecting the study of the network. With these assumptions, from the molecular weight per arm M_{arm} and the total mass density we obtained the number density of stars ρ. Next we need a method to determine the Likos parameter σ in eq 2. Since we are dealing with a polymer melt, we know that the calculated number density applies to a system at a pressure of 1 atm. Given that the Rouse arms do not contribute to the pressure, we performed several simulations with the correct number density and temperature and varied the value of σ until we obtained a pressure of 1 atm. This resulted in σ = 6.1 nm.

Although the above monodispersity assumptions have little or no influence on the modeling of the precursor, they may have a larger influence on describing the dynamics of the network. An appropriate way to prepare networks would be to generate a precursor system by sampling from some appropriate distribution of functionalities and arm lengths, next allow for cross-linking as described below, and finally average calculated shear relaxation moduli over many such boxes until reasonable statistics would be obtained. As we will see below, it takes at least ten runs per monodisperse system to obtain reasonable statistics, which makes an ensemble average as just mentioned computationally prohibitive. We therefore decided to stick to the monodisperse system already used for the precursor. Moreover, we assume that on average one sticker group per arm will be active.

We now turn to the parameters in the Rouse part of the potential. The spring constant can be calculated when the Kuhn length is known. We used a Kuhn length b of 4 nm as cited for poly nBA by Pahnke et al.[61] This yields a spring constant $k_s = 6.67 \times 10^{-4}$ N m^{-1}. The final remaining unknown is the number of Kuhn segments, or beads, per arm N. To obtain this number, we first estimate the average end-end length R_{arm} of a polymer arm. Since the Likos potential is basically the entropy loss of two stars when they overlap, it must have decayed to zero when the distance between them is roughly twice the average end-end length of an arm. By looking at the potential in Figure 2, we see that above $R_c = 3.5\sigma$ the potential has decayed to an insignificant value, from which it follows that $3.5\sigma = 2R_{arm} = 2\sqrt{Nb}$. This leads to R_{arm} = 10.6 nm and N = 7. $R_c = 3.5\sigma$ has been used as a cutoff radius for the Likos potential.

Obviously, the procedure that we have applied to obtain R_{arm} and N depends quite a bit on the chosen value of R_c. Reasonable choices of R_c lead to numbers of beads per arm ranging from six to eight. Moreover, we want to mention that a Kuhn length of 4 nm seems to be quite large but that none of the qualitative results below will change if a smaller Kuhn length is used. The only difference will be that the agreement between experimental and simulated shear relaxation moduli will be extended to somewhat smaller times.

All simulation parameters mentioned so far are given in Table 1, together with two friction parameters appearing in the propagators. The friction parameters have been adjusted to obtain the best possible agreement between theoretical and experimental shear relaxation moduli. One of them is ξ_c, the friction on the cores. Below it will turn out to be equal to 7.6×10^{-3} kg/s. The other is ξ_0, occurring in the Rouse mode dynamics through $w = k_s/\xi_0$, which will turn out to be 9.45×10^{-8} kg/s. Various ways to define the m_n will be discussed later. From its molecular mass, we determine that the DSDMA sticker group is approximately one-sixth of the mass of each Kuhn bead in the arms.[39] As mentioned before, when creating loops and bridges, we lump together the two sticker groups that form the bond into one bead, leading to chains of $2N + 1$ beads, with the middle bead having a friction equal to one-third of a normal bead at that position.

DOI: 10.1021/acs.macromol.7b02613
Macromolecules 2018, 51, 2872−2886

Table 1. System Parameters

parameter		value
butyl acrylate	M_w	128.17 g mol^{-1}
DSDMA	M_w	290.4 g mol^{-1}
mass per arm	M_{arm}	16662 g mol^{-1}
functionality	f	13
Kuhn length	b	4 nm
mass density	ρ_{mass}	1.06 g cm^{-3}
temperature precursor	T_{prec}	258 K
temperature gel	T_{netw}	273 K
number density	ρ	2.959×10^{24} m^{-3}
number of particles	N_t	300
box length	L_{box}	46.7 nm
Likos parameter	σ	6.1 nm
cutoff radius	R_c	21.2 nm
number of beads per arm	N	7
spring coefficient	k_{spring}	6.67×10^{-4} N m^{-1}
core friction	ξ_c	7.60×10^{-3} kg s^{-1}
reference bead friction	ξ_0	9.45×10^{-8} kg s^{-1}

Assuming that the cores should not move by more than one-twentieth of the radius of the stars, we find that the time step dt should at most be equal to $(R_{arm}/20)^2\xi_c/k_BT$, which is equal to 0.5 s. This is roughly confirmed from calculations of the mean-square displacements shown in Figure 4, where it is seen that dt must be less than one-tenth of a second to capture subdiffusive behavior.

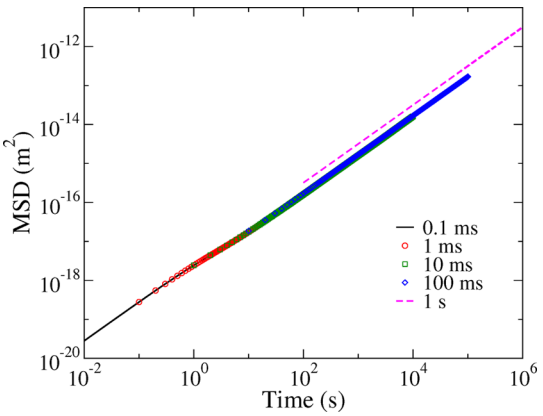

Figure 4. Mean-square displacements of the core for various time steps. The dashed line, corresponding to a time step of 1 s, does not reproduce the correct diffusive behavior, and thus is too large to obtain reliable results. The maximum time step used in this study is 10 ms.

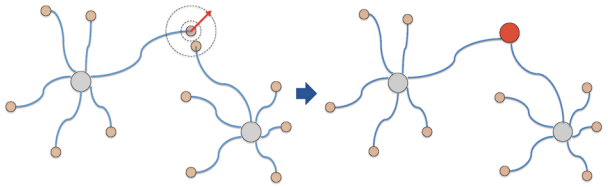

Figure 5. Schematic of two sticker groups binding. The central red bead in the right part represents the merger of the groups to form one bead of twice the mass.

3.3. Creation of Networks. Our main interest in this paper is the relation between the degree of cross-linking in the network and its rheological properties. To quantify cross-linking, we introduce a parameter p_{ext}, defined as the number of stickers involved in external bonds divided by the total number of stickers and next multiplied by 100. This is the same as the total number of external bonds divided by the total number of possible bonds, also multiplied by 100. For short, we will call it the percentage of external bonds. In a similar way we define the percentage of loops and the percentage of dangling chains, the latter being just the percentage of all stickers that are not involved in any bond. Since the contribution of a loop to the shear relaxation modulus is not very different from that of (two) dangling chains, at least compared to the changes that will occur on creating bridges, from now on we will not discriminate between the two and restrict ourselves to systems that have prescribed values for p_{ext}. For stars with very long arms this may not hold true anymore, but then also modeling the arms by Rouse chains will become invalid.

In order to generate cross-linked networks, we attached an additional eighth bead with one-sixth the friction of a regular bead to the end of each arm of the precursor, the factor of one-sixth being roughly estimated on the basis of the relative sizes of the sticker with respect to the Kuhn length. Next the system was equilibrated in the usual way. After this preliminary run, the sticking procedure was started. To this end, we ran the system with a time step of 1 ms and included a sticking step after every 100 steps. During the sticking step, for every sticker, we scanned a spherical volume of one-tenth of a Kuhn length and formed a bond to the nearest-neighbor in this volume. The run was stopped as soon as a prescribed value for p_{ext} was obtained. In our case, one-tenth of a Kuhn length corresponds to a few angstroms. Moreover, the sticking probability in this case is rather small, so the total runtime for creating a box lasted long enough for the cores to diffuse over about one diameter.

In order to further reduce the statistical noise in our final results, ten boxes were created for each value of p_{ext}, and the final shear relaxation moduli were obtained by averaging over these ten boxes. Moreover, in each case three runs were performed with time steps of 0.1, 1, and 10 ms in order to resolve all time scales from the smallest, allowed by the coarseness of the model, to the longest, needed to reach the plateau values of the shear relaxation moduli.

3.4. Methods. *3.4.1. Rheological Experiments.* The linear viscoelastic responses were probed by small-strain amplitude oscillatory shear measurements with an ARES-2KFRTN1 strain-controlled rheometer equipped with a force rebalance transducer (TA Instruments, USA). The TTS principle was applied to build master curves at the reference temperature of $T_{ref} = T_g + 44$ °C for all the samples, where T_g is the glass transition temperature of the sample considered. The reference temperatures for the precursor and the network were chosen in order to compare both sets of data at the same distance from their respective T_g (please see Supporting Information). For the precursor this amounts to $T_{ref} = -15$ °C and for the network to $T_{ref} = 0$ °C. 8 mm Invar parallel plates with low expansion coefficient were used and reproducibility of the measurements was checked by going down in temperature by a step of 10 °C as a first measurement and up to check the reproducibility of the data at 2 or 3 temperatures (see Supporting Information for details).

3.4.2. Simulation. Simulated stresses were obtained according to

$$\sigma_{xy}(t) = -\frac{1}{V}\sum_j\sum_i (r_{ix}(t) - r_{jx}(t))F_{ij,y}(t) \quad (18)$$

where $F_{ij,y}(t)$ is the y-component of the force exerted by particle j at position $\vec{r}_j$ on particle i at position $\vec{r}_i$. By particle, we mean either core or bead. The shear relaxation modulus $G(t)$ was calculated according to

$$G(t) = \frac{V}{k_BT}\langle\sigma_{xy}(t)\sigma_{xy}(0)\rangle \quad (19)$$

Applying these equations to the Rouse model leads to the well-known result

$$G(t) = \nu k_BT\sum_{k=1}^{N_s} e^{-6(k_BT\lambda_k/\xi_0 b^2)t} \quad (20)$$

where λ_k is the kth eigenvalue of the Rouse matrix. Here N_s stands for the number of Kuhn segments being considered; for dangling arms this is N and for bridges $2N + 1$.

DOI: 10.1021/acs.macromol.7b02613
Macromolecules 2018, 51, 2872−2886

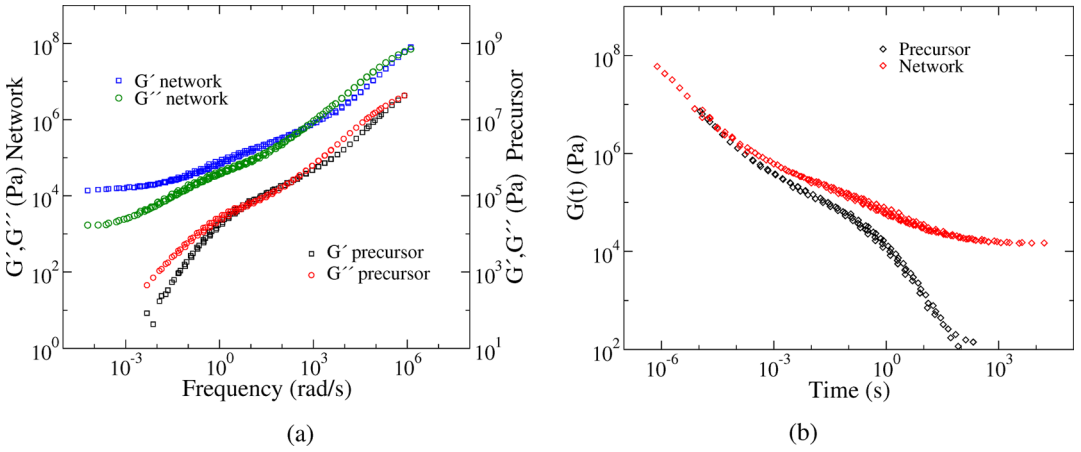

Figure 6. (a) Shear relaxation moduli obtained from experiment both for the precursor and for the cross-linked network. The terminal plateau at low frequencies is an indication of gelation. Two different *y*-axes are used to clearly distinguish between the two sets of moduli. (b) The corresponding $G(t)$ for both the network and precursor. The time domain moduli are easier to work with for simulations.

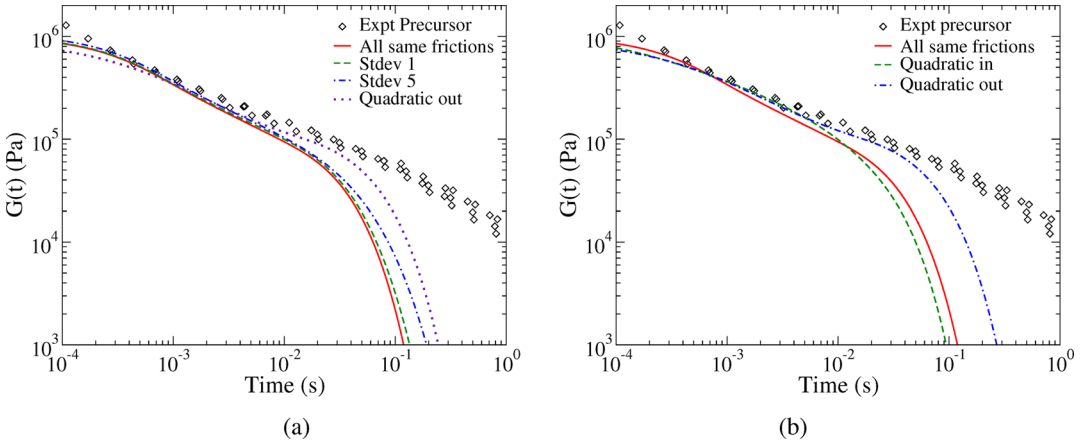

Figure 7. (a) Effect of polydispersity on stress relaxation. Arms sampled from a Gaussian distribution with standard deviation 1 (dashed line) and standard deviation 5 (dash-dotted line) relax later than the solid line. Also shown is the quadratic-out result (dots, same as dash dotted line in the panel b. (b) Quadratic friction model with friction increasing quadratically toward the core (dashed line) or outward (dash-dotted line).

4. RESULTS

In Figure 6a, we present the storage and loss moduli $G'(\omega)$ and $G''(\omega)$ obtained with the strain-controlled rheometer mentioned in section 3.3, both for the precursor and for the network. Using the method of Schwarzl,[62] we transformed these data into "experimental" shear relaxation moduli shown in Figure 6b. We refer the reader to the Supporting Information for the raw data and some additional discussion concerning the application of the TTS principle. At intermediate and lower frequencies TTS becomes increasingly difficult, especially in associating systems and may fail eventually.[33]

On the basis of extensive experience with similar systems, we have concluded that the Schwarzl method[62] is superior to the other methods available. This is confirmed in a paper by Emri et al.,[63] who especially address this issue.

4.1. Rheology of the Precursor. We first discuss the results for the precursor.

As already mentioned before, the motion of the cores is much slower than that of the Rouse beads, so the early decay of the shear relaxation modulus is totally determined by the Rouse dynamics. Moreover, at early times, the contribution of the core−core interactions to the shear relaxation modulus is negligibly small compared to those of the Rouse modes. We therefore neglect at this stage the contribution of the core−core interactions to the stress and completely concentrate on the Rouse dynamics. As we have already determined the bead density, the plateau value of the Rouse contribution is fixed, and we should only decide about the best possible friction model and corresponding parameters. As a first try, we used a simple isofrictional model. The best result was obtained using a friction value of $\xi = 1.89 \times 10^{-6}$ kg s^{-1} (for all beads). The corresponding shear relaxation modulus is shown in Figures 7a and 7b as a red curve, together with the experimental curve. It is clear that the agreement is reasonably good, but not perfect. In particular, the slope of the theoretical curve is different from that of the experimental curve.

In view of the polydispersity of the experimental system (section 3.1 and Supporting Information), we tried to ameliorate the quality of the Rouse model prediction by including polydispersity. As already mentioned, we only needed to calculate the contribution to the shear relaxation modulus of individual arms of various lengths, average the result over a reasonable distribution of arm lengths, and multiply by 13 (the nominal number of arms per star). We used discrete Gaussian distributions with given standard deviations. To be more explicit, we calculated the Rouse prediction for arms attached to a fixed point with the arm length running from 4 to 11 Kuhn

DOI: 10.1021/acs.macromol.7b02613
Macromolecules 2018, 51, 2872−2886

beads, took relative weights for each arm length from a Gaussian distribution with mean of 7 Kuhn beads and the given standard deviation, and averaged over the chosen weights; this result was finally multiplied by 13. The result is shown in Figure 7a for two values of the standard deviation. With all standard deviations ≥5 we found the same result. It is seen from this plot that including polydispersity does extend the relaxation to somewhat larger time scales, for obvious reasons, but does not change the slope of the curve (in a log−log representation). We therefore decided to stick to monodisperse arm lengths and focus on frictions in order to obtain a better model.

Since it is conceivable that frictions on different beads along the arms may differ substantially, we investigated if better agreement can be obtained using models with nonuniform frictions. In order to clearly see the influence of the various friction models, we decided to keep the total friction on each arm constant, i.e. we chose all models such that $\sum_{i=1}^{7}\xi_i = 13.23 \times 10^{-6}$ kg s^{-1}.

First, we applied a model with frictions increasing or decreasing linearly with bead number. The model with frictions increasing toward the free end slightly improved the results. We next tried several other models and found good results with a model in which the bead friction grows quadratically with the bead number: $\xi_i = \xi_0 \times i^2$. The only unknown, ξ_0, follows from the constraint of constant total friction introduced earlier; its value is given in Table 1. The results are depicted in Figure 7b along with those of a model for which $\xi_i = \xi_0' \times i^{-2}$ for comparison. Clearly, the model with quadratically outward growing frictions does a very good job, while the one with quadratically inward growing frictions obviously does not describe the data as well. Even though this result may be a bit counterintuitive we continue with this friction model, leaving a more detailed analysis with different models for future research.

Up to now, we have only been concerned with the Rouse dynamics of the model that determines the early decay of the shear relaxation modulus. We now add the contributions from the core−core interactions and vary the value of the core friction ξ_c to obtain the best agreement between theory and experiment. The final result is presented in Figure 8, for which $\xi_c = 7.60 \times 10^{-3}$ kg s^{-1}. We notice that the agreement is good, given the fact that apart from the two frictions, shifting the two contributions along the horizontal axis, all parameters were obtained from considerations totally independent of the rheological data.

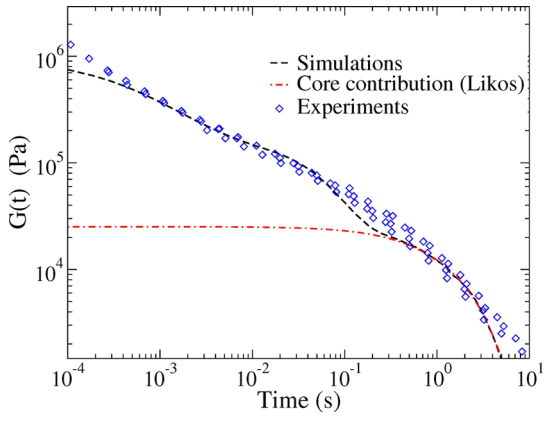

Figure 8. Best fit (dashed line) to the precursor experimental $G(t)$ (symbols). The contribution of the potential of mean force is shown separately (dash-dotted line). In the simulation model the bead friction increases quadratically along the arms of the star.

Whereas the agreement is good enough for our purposes (given the simplicity of the model and the approximations used), one might argue that the final shear relaxation modulus appears to relax in a one-step, rather than a two-step process, as also suggested by the experiment. In this context, we recall that the Kuhn length of 4.0 nm, as inferred from data in the literature seems to be quite large. However, if we consider a model with a Kuhn length half of that, we end up with more Kuhn beads (28). As a result, the shear relaxation function starts at a larger value at time zero and extends slightly to longer times. The latter can be made more pronounced by using a polydisperse model which includes arm lengths up to 45 beads. This partially fills the gap between the time scales of the Rouse modes and the core dynamics, thereby smoothing out the two-step character mentioned above. Since our main goal is to provide a sound distribution of stickers before starting the relaxation process, we did not investigate these possibilities further. This is worth investigating in the future.

Before finishing this section, let us discuss the meaning of "core" a bit further. By "core" we do not just mean the chemical unit that has been used to attach the arms to (see section 3.1). After attaching the arms, the central region of the star will be rather crowded. In a realistic model, based on Kuhn beads including mutual repulsions, this means that it will be difficult for two stars to approach each other closer than a certain distance. This distance may be considered to be the core diameter and has to be calculated. From the radial distribution function in Figure 2 we find that no stars come closer than 0.5σ, so we could define the diameter to be 0.5σ. This of course seems like a gross underestimation. A better choice obviously is to notice that according to Boltzmann statistics, stars will hardly ever come closer to each other than distances for which the mutual interaction energy is less than, let us say, $10k_BT$. This leads to a diameter of about 1σ and a corresponding volume fraction of about 0.39. Consequently, the cores still have plenty of space to move. The same conclusion follows from the fact that the value of the first peak of the scattering function (structure factor), which is not shown, equals 1.33, well below the value of 2.85 where according to the Hansen−Verlet rule[64] the system crystallizes. The picture now is that of a collection of cores in a sea of arms. The sea of arms in a real system is a rather complicated, dense fluctuating liquid. It will cause a large, probably distance dependent, friction on the cores, leading to rather slow motions and corresponding stress relaxation of the cores. The slowness of the cores is just a reflection of the complicated motion of the arms that is not fully captured by the Rouse model.

It may be useful to notice that although the contribution of the core to the stress relaxation is the slowest in the system, its stress value is the smallest, and hence its contribution to the viscosity is rather modest. As a result, one may conclude that the viscosity of the star systems is dominated by the lengths of the arms, rather independent of the functionality. This result has been confirmed for entangled stars with experiments and tube model theory but only for functionalities not exceeding 32.[65−67]

4.2. Network. After having studied the precursor, we added a sticker to the arms of the stars, making them telechelic, and proceeded to generate a network.[39] We measured the rheological response of the resulting network with our strain-controlled rheometer. The results are shown in Figure 6a. As

DOI: 10.1021/acs.macromol.7b02613
Macromolecules 2018, 51, 2872−2886

with the precursor, we transformed the data into $G(t)$ by means of the method of Schwarzl.[62] The resulting "experimental" $G(t)$ is shown in Figure 6b together with the one of the precursor. The first thing to notice is that both curves agree at times below about 10^{-5} s, after which they begin to differ substantially. For times larger than 10^3 s the modulus of the network reaches a plateau value, caused by the network structure.

Before continuing with a discussion of the rheological results, let us quickly sketch how the motion of the cores is influenced by the introduction of bridges. In Figure 9, we have plotted the mean-square displacements of the cores in networks for various values of p_{ext}. It is clearly seen that in the network the mean-square displacements of the cores level off beyond times of about 100 s, depending somewhat on the degree of cross-linking. It is clearly seen that the cores explore a volume with a diameter of about 1 or 2 times the radius of a star, even for cross-link percentages of 60% to 80%. So, at lower cross-link percentages, it may be expected that all cores, including those in star clusters, have the freedom to move over about one diameter.

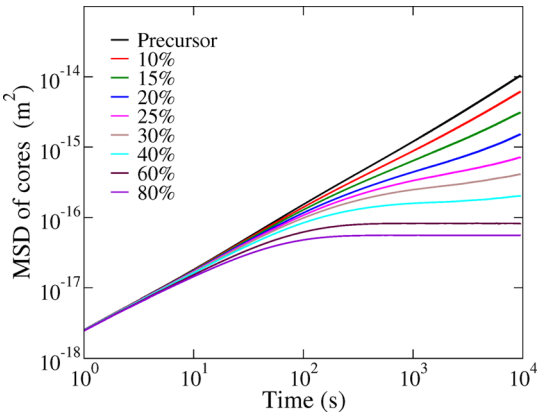

Figure 9. Mean-square displacement (MSD) of the cores with increasing cross-link percentage. The MSD decreases with increasing p_{ext}, showing that the cores find it increasingly difficult to move with higher degrees of cross-linking. This slowing is due to the tethering effect of the bridge chains between cores.

It is not fully clear what causes the slowing down of the network in the intermediate region, indicated by the difference of the slopes of the two curves. One might argue that cross-linking the stars has resulted in topologies of the arms in which some of them are constrained to slide along others in order to relax stresses whose removal requires larger displacements of the beads then needed to relax short-range stresses. Another point of view might be that there is a distribution of clusters (of connected stars), each contributing with their own characteristic relaxation times, which increase with increasing cluster sizes.

An important aim of our simulations is to shed light on these matters. Moreover, we wish to establish the degree of cross-linking in the system.

In order to allow for reasonable statistics with the simulated results, we prepared ten boxes of cross-linked systems for a range of cross-link percentages p_{ext}. Since the bond energy of a sulfur−sulfur bond[68−70] is about 250 kJ mol^{-1}/R ≈ 30 000 K, where R is the gas constant, the lifetime of a bond is extremely long, and fluctuations caused by association and dissociation can safely be ignored. Since the network response spans several decades in time, we ran each of these boxes for three different timesteps of 0.1, 1, and 10 ms and then merged the resulting shear relaxation moduli into one smooth curve. The results of all these calculations are shown in Figure 10a, together with the experimental curve. As is clear from this picture, the simulated results meet the experimental data very well when a cross-linking percentage of 25% is assumed. In Figure 10b, we present the simulated $G(t)$ again, but now together with $G(t) \pm \sigma_{st}(t)$, where $\sigma_{st}(t)$ is the standard deviation of the average obtained with the ten simulation boxes. Comparing Figure 10a with Figure 10b, it seems safe to say that the actual cross-link percentage is 25 ± 10%.

There is a second way to estimate the actual p_{ext}. With increasing cross-linking, the terminal plateau seems to converge to a value of about 70 kPa for a fully cross-linked network (confirmed by simulations with larger p_{ext}, not shown to save the picture from becoming unreadable). This result is in

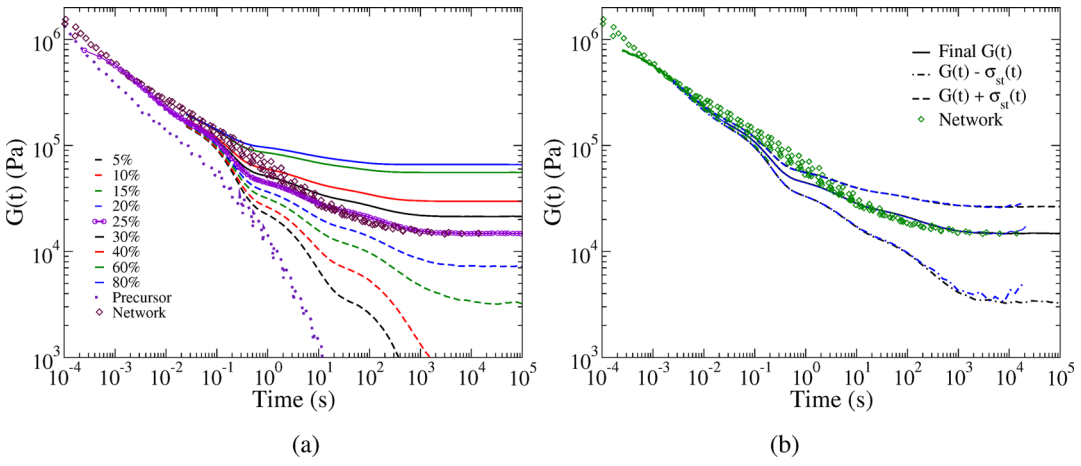

Figure 10. (a) Stress relaxation moduli for various cross-link percentages. The terminal plateau, which first appears at 15%, keeps increasing with increasing degrees of cross-linking. The model with 25% of maximum cross-linking describes the experimental modulus best. (b) Stress relaxation modulus for 25% of maximum cross-linking along with two curves—one standard deviation above (dashed line) and one below (dash-dotted line) average. Each of the latter two is represented twice—once for a run with a short time step and once for a run with a larger time step. Besides these, in both figures the experimental curve is shown.

DOI: 10.1021/acs.macromol.7b02613
Macromolecules 2018, 51, 2872−2886

agreement with an estimate suggested by van Ruymbeke et al.[34] According to these authors, the maximum cross-link percentage is given by $\nu_{max} = \rho_m N_{Av}/2M_a$, where ρ_m is the mass density of stars, N_{Av} is the Avogadro number, and M_a = 16.6 kg/mol the mass of one arm (including the sticker). With the Green–Tobolsky relation $G_{max} = \nu_{max} k_B T$ one again obtains G_{max} = 70 kPa. Now, with an experimental plateau value of about 14 kPa and the proportionality of the plateau value to the cross-link percentage, we conclude that the degree of cross-linking is about 20%, in reasonable agreement with the previous estimate.

It is worth reflecting as to why the percentage of all possible cross-links that finally materialize is so low. As is clear from the binding energy of a disulfur bond, 30 000 K, this cannot be due to reversible association and dissociation of the bonds. From the description of the synthesis, however, it is clear that some arms may have no sticker groups while others may have more than one. Also, two out of three fingers at the end of an arm can become inactive by intrasticker association. This will influence the efficiency with which cross-links can be formed. Similarly, during the cross-linking process sticker groups must diffuse over substantial distances to find possible partners. This becomes increasingly more difficult with increasing degree of cross-linking already established, so stickers may finally get kinetically trapped in regions with few or no free partners. This also means that after annealing at elevated temperatures the percentage of cross-linking may slightly have gone up. Note that this is contrary to the effect of temperature with lower association energies, when a reversible association dissociation equilibrium is established.

We now turn our attention to the intermediate time scales between 10^{-5} and 10^{2} s. In order to obtain good agreement between our simulated results and the experimental data at times shorter than 10^{-5} s, we have multiplied all frictions by a constant factor of 2.65, no other modifications being applied. From this we draw two conclusions: First, the fact that the friction of the beads in the network is much larger than those in the precursor agrees with our earlier hypothesis that cross-linking the system results in topologies with enhanced friction when chains move in order to relax their stresses. This, of course, is not reproduced by phantom chains and therefore had to be introduced by hand. Second, the fact that no further changes of relative frictions are needed confirms that the remaining slowing down, indicated by the smaller frequency slope of moduli for the network than for the precursor, is indeed reproduced by our phantom chains. It must therefore be a result of the distribution of cluster sizes occurring in the cross-linked system, as suggested before.

Stresses in the network again consist of two components: one due to entropic interactions between stars, described by the potential of mean force, and the other due to Rouse springs. The first contribution is small in magnitude but plays an important role in keeping the stars apart, and its relaxation is roughly identical to that of the precursor shown in Figure 8 for all the different cross-link percentages. Only for cross-link percentages of 60% or more the relaxation becomes slightly slower than that of the precursor. Given their non-negligible size, it may be a bit surprising that the Likos forces do not contribute to the final plateau. The reason for this is that their actual volume fraction is rather small. The connection to other cores through rather flexible Rouse arms is also not very restrictive topologically. Therefore, as we have seen above, the cores have plenty of space to wiggle around, thereby reducing their contribution to the stress correlation. Of course, since the cores are now part of a physical network, they cannot diffuse over all space anymore, but the remaining space is sufficient to allow for core–core stress relaxation, without the need (or possibility) to hop from one cage to another. These considerations do not mean that the cores do not contribute to the final plateau. Being part of the network, and as such experiencing forces generated by the Rouse part of the Hamiltonian, eq 7, the cores do contribute to the stresses and stress relaxations of the network. This is the part that we call "the Rouse part" of the stress relaxation.

The Rouse part, dominating in all cases and shown in Figure 11 for the largest time step of 10 ms, has some interesting

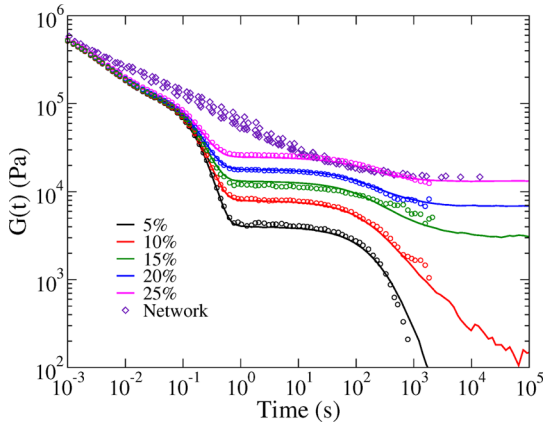

Figure 11. Rouse contribution to stress relaxations for networks of increasing degree of cross-linking. All curves enter a "Rouse" plateau at about 0.3 s. With cross-link percentages of 15% and onward they develop a second plateau, which increases and merges with the first plateau with increasing cross-linking. $G(t)$ for 10% of full cross-linking clearly has a power law tail. Circles are obtained with runs of time step 0.1 ms and solid lines with a time step of 10 ms.

characteristics. For all cross-link percentages, there is an onset of a second plateau at 0.3 s. For 5 and 10% pregel states, this plateau eventually decays. The magnitude of the plateau increases with cross-link percentages and eventually segues into the terminal plateau when gelation occurs at about 15% in the figure. For percentages higher than 30%, there is one single plateau due to the whole system being interconnected.

We now analyze the onset of gelation as much as is allowed by the statistics of our data. Increasing the cross-link percentage starting with 5.5%, below which the terminal part of $G(t)$ decays exponentially to zero, $G(t)$ develops a tail, which roughly may be described by a power law $G(t) \propto t^{-\alpha}$. In Figure 12a, we present these tails together with the suggested power law descriptions for cross-link percentages ranging from 9% to 10.5%. At 11%, $G(t)$, instead of decaying, enters a terminal plateau region, described by $\alpha = 0$. Beyond this point the system finds itself in the gel state. For higher percentages, the value of the terminal modulus increases as reported earlier. The exponents of the power law, α, are plotted in Figure 12b. Included in this figure is a fit of the data according to $\alpha(p_{ext}) = A(p_G - p_{ext})^{\beta}$, which yielded A = 0.5283, p_G = 10.55%, and the exponent β = 0.3895. We conclude that the gelation occurs at about p_G = 10.55%. It is tempting to call β a critical exponent associated with the gel transition, even when this may not be fully justified, since there is no variable in the system which is thermodynamically conjugate to p_{ext}. Notice that the various p_{ext} were obtained by just freezing them in.

DOI: 10.1021/acs.macromol.7b02613
Macromolecules 2018, 51, 2872–2886

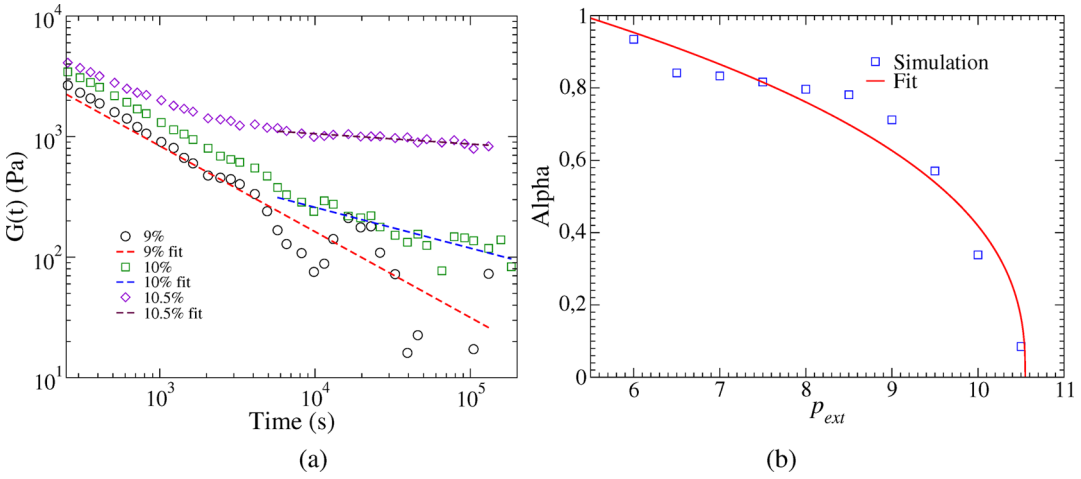

Figure 12. (a) Appearance of a power law tail with $G(t)$'s for 9%, 10%, and 10.5% of maximum cross-linking; the dashed straight lines represent the suggested power laws. (b) Power law exponents α of the terminal parts of $G(t)$ as a function of percentage of maximum cross-linking (squares) and fit revealing the gelation point at 10.55% of maximum cross-link percentage (solid line).

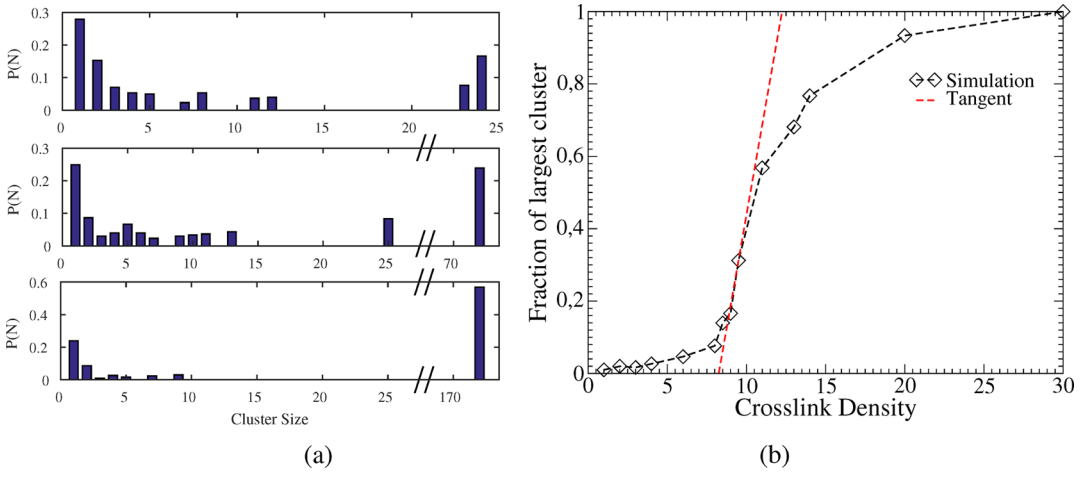

Figure 13. (a) Distribution of cluster sizes for 9%, 10%, and 11% of maximum cross-linking. The rightmost bar in the middle and bottom panes after the x-axis break represents the size of the largest cluster. At 10% of maximum cross-linking about 25% of all stars in the sample are in this big cluster, which number increases to 50% at 11% of maximum cross-linking. (b) Fraction of the largest cluster in the sample as a function of percentage of maximum cross-linking. The tangent at the inflection point intersects the line $y = 1$ at 12.5% of maximum cross-linking.

It is clear that the onset of gelation may be attributed to the appearance of a so-called "giant component", which is one very large cluster that connects or spans the whole system. In order to explore this point, we made histograms of the distribution of cluster sizes in the system.

Figure 13a shows the distributions of the cluster sizes, in terms of the fraction of stars $P(N)$ that find themselves in clusters of size N (not the bead number here), which is represented along the x-axis. First, consider the top panel of Figure 13a which shows the cluster size distribution at 9% of maximum cross-linking. Most stars in the system are unconnected, represented by the bar at 1 on the extreme left. The largest cluster at the extreme right has 24 stars. From the figure we read $P(24) = 0.16$, from which we conclude that there are $0.16 \times 300/24 = 2$ clusters of size 24. At 10%, shown in the middle panel, the biggest cluster increases in size, to include 72 stars. The corresponding bar is the rightmost one, after the axis break. From the figure we read $P(72) = 0.24$, so there is only one largest cluster in this case, which takes about 25% of all stars in the box. There is still a substantial fraction of unconnected stars and clusters of varying sizes up to a maximum of 25. However, with just a 1% increase of the cross-link percentage, at 11%, the situation is quite different. From the bottom panel of Figure 13a, we notice a substantial change of the structural properties of the system. The rightmost bar is now dominant and represents one giant cluster of 172 stars, which is a little over 50% of the total number of stars in the system. The proportion of unconnected stars has reduced a lot, and the sizes of the small clusters now range only up to nine. The big component has come to existence by eating the small clusters. As the sticking percentage is increased, this cluster continues to grow, as shown in Figure 13b, where the fraction of stars in the largest cluster is plotted as a function of the cross-link percentage. First of all, this analysis shows that gelation is strongly related to the growth of the largest cluster in the system, as expected. Second, the largest cluster does not yet span the whole system at the cross-link percentage where according to rheology gelation takes place. One procedure to extract a p_G from this data might be to draw the tangent line to the curve at the inflection point and read the value of p_{ext} where this line crosses unity. This procedure leads to a value of p_G = 11−12%, in rough agreement with the rheology-based value.

DOI: 10.1021/acs.macromol.7b02613
Macromolecules 2018, 51, 2872−2886

This analysis shows the connection between the statistics of the clusters and the onset of the power law tail in the $G(t)$. It is clear from Figure 12a that at 10% of full cross-linking a power law tail in $G(t)$ has developed. At the same time, we see the appearance of a large cluster represented by the rightmost bar in the middle panel of Figure 13a. This was a feature that was observed in all 10 simulation boxes. With increasing p_{ext} both the size of the large cluster increases, and the power law decay slows down. We checked that p_G obtained with the structural analysis is equal in boxes with 300 stars and boxes with 1000 stars.

5. SUMMARY AND CONCLUSIONS

In this paper, we have studied the rheological and gelation properties of a star polymer melt consisting of telechelic stars with 13 arms of seven Kuhn segments each, both using experimental and simulation methods. First, we studied the non-cross-linked precursor and next cross-linked networks of various degrees of cross-linking. The agreement between theory and experiment is very good. This allowed us to analyze the origin of the gel transition in some detail, using our simulation techniques.

As usual with soft matter systems, the information about molecular properties of the various constituents of the system is rather limited. For example, knowing the hydrodynamic radius of the molecule is of little help when it comes to deciding about the structure of the molecule in the melt. Here we decided to use a thermodynamically consistent model in which the stars are treated as point particles dressed with phantom, or Rouse chains. Forces between the point particles are governed by the potential of mean force, which we modeled with a function that has extensively been used by Likos and co-workers. Adjusting the only unknown parameter in this function until the pressure of the system was equal to 1 atm, we managed to fully determine the potential of mean force. Since only the Kuhn length was known, but not the mass of the corresponding segment, we estimated the length of the arms by simply choosing a cutoff for the potential of mean force and equating this to twice the length of an arm. The results in this paper seem to fully justify this procedure. Even so, the suggested procedure is not uniquely defined and in other cases may even not be applicable at all. In those cases independent information, like for example from SAXS or other scattering experiments will be of great help.

The remaining parameters in the model are the friction coefficients for the cores and for the Rouse beads. These were adjusted to obtain agreement between theory and experiment for the precursor system. In order to obtain good agreement, it turned out to be necessary to assume that the frictions on the beads depend on their position along the arms. It turned out that a model in which the friction increases quadratically with the bead number along the arm, starting with one for the bead connected to the core, does a perfect job. We derived the exact Rouse dynamics for cases with variable frictions in order to be able to use large time steps needed to reach the extremely long decay times of the shear relaxation moduli, also in the case of cross-linked networks.

We created and simulated cross-linked networks with various degrees of cross-linking. Without any further parameter tweaking, i.e., just using the parameters obtained for the precursor, we found that simulations with 25% of all the arms involved in cross-links to other stars yield shear relaxation moduli in very good agreement with the experimental results. We analyzed the long time tails of the shear relaxation moduli for systems approaching the gel transition and found algebraic decays with exponents decaying to zero as also observed with thermodynamic properties of systems near second-order phase transitions. We confirmed that the gel transition is strongly related to the growth of the largest cluster in the system.

■ ASSOCIATED CONTENT

Supporting Information

The Supporting Information is available free of charge on the ACS Publications website at DOI: 10.1021/acs.macromol.7b02613.

Sythesis details and protocols of experimental rheology (PDF)

■ AUTHOR INFORMATION

Corresponding Author

*E-mail: v.metri@utwente.nl (V.M.).

ORCID

Vishal Metri: 0000-0002-5291-4416

Jiajun Yan: 0000-0003-3286-3268

Guilhem P. Baeza: 0000-0002-5142-9670

Krzysztof Matyjaszewski: 0000-0003-1960-3402

Notes

The authors declare no competing financial interest.

■ ACKNOWLEDGMENTS

The work leading to these results has received funding from the People Programme (Marie Skłodowska-Curie Actions) of the European Union's Seventh Framework Programme (FP7/2007-2013) under REA grant agreement no. 607937−SUPOLEN project. Support from NSF (DMR 1501324) is gratefully acknowledged.

■ REFERENCES

(1) Brunsveld, L.; Folmer, B.; Meijer, E. W.; Sijbesma, R. Supramolecular polymers. *Chem. Rev.* **2001**, *101*, 4071−4098.

(2) Seiffert, S.; Sprakel, J. Physical chemistry of supramolecular polymer networks. *Chem. Soc. Rev.* **2012**, *41*, 909−930.

(3) Gold, B.; Hövelmann, C.; Lühmann, N.; Pyckhout-Hintzen, W.; Wischnewski, A.; Richter, D. The microscopic origin of the rheology in supramolecular entangled polymer networks. *J. Rheol.* **2017**, *61*, 1211−1226.

(4) Louhichi, A.; Jacob, A.; Bouteiller, L.; Vlassopoulos, D. Humidity affects the viscoelastic properties of supramolecular living polymers. *J. Rheol.* **2017**, *61*, 1173−1182.

(5) Chen, Q.; Huang, C.; Weiss, R.; Colby, R. H. Viscoelasticity of reversible gelation for ionomers. *Macromolecules* **2015**, *48*, 1221−1230.

(6) Brassinne, J.; Fustin, C.-A.; Gohy, J.-F. Polymer gels constructed through metal−ligand coordination. *J. Inorg. Organomet. Polym. Mater.* **2013**, *23*, 24−40.

(7) Van Ruymbeke, E. Preface: Special Issue on Associating Polymers. *J. Rheol.* **2017**, *61*, 1099−1102.

(8) Michal, B. T.; Jaye, C. A.; Spencer, E. J.; Rowan, S. J. Inherently photohealable and thermal shape-memory polydisulfide networks. *ACS Macro Lett.* **2013**, *2*, 694−699.

(9) Hu, J.; Zhu, Y.; Huang, H.; Lu, J. Recent advances in shape−memory polymers: Structure, mechanism, functionality, modeling and applications. *Prog. Polym. Sci.* **2012**, *37*, 1720−1763.

(10) Maes, F.; Montarnal, D.; Cantournet, S.; Tournilhac, F.; Corté, L.; Leibler, L. Activation and deactivation of self-healing in supramolecular rubbers. *Soft Matter* **2012**, *8*, 1681−1687.

(11) Sordo, F.; Mougnier, S.-J.; Loureiro, N.; Tournilhac, F.; Michaud, V. Design of Self-Healing Supramolecular Rubbers with a

DOI: 10.1021/acs.macromol.7b02613
Macromolecules 2018, 51, 2872−2886

Tunable Number of Chemical Cross-Links. *Macromolecules* **2015**, *48*, 4394−4402.
(12) Yan, T.; Schröter, K.; Herbst, F.; Binder, W. H.; Thurn-Albrecht, T. Unveiling the molecular mechanism of self-healing in a telechelic, supramolecular polymer network. *Sci. Rep.* **2016**, *6*, 32356.
(13) Cordier, P.; Tournilhac, F.; Soulié-Ziakovic, C.; Leibler, L. Self-healing and thermoreversible rubber from supramolecular assembly. *Nature* **2008**, *451*, 977−980.
(14) Schmolke, W.; Perner, N.; Seiffert, S. Dynamically Cross-Linked Polydimethylsiloxane Networks with Ambient-Temperature Self-Healing. *Macromolecules* **2015**, *48*, 8781−8788.
(15) Skrzeszewska, P. J.; Sprakel, J.; de Wolf, F. A.; Fokkink, R.; Cohen Stuart, M. A.; van der Gucht, J. Fracture and self-healing in a well-defined self-assembled polymer network. *Macromolecules* **2010**, *43*, 3542−3548.
(16) Kolmakov, G. V.; Matyjaszewski, K.; Balazs, A. C. Harnessing labile bonds between nanogel particles to create self-healing materials. *ACS Nano* **2009**, *3*, 885−892.
(17) Long, R.; Mayumi, K.; Creton, C.; Narita, T.; Hui, C.-Y. Rheology of a dual crosslink self-healing gel: Theory and measurement using parallel-plate torsional rheometry. *J. Rheol.* **2015**, *59*, 643−665.
(18) Yoon, J. A.; Kamada, J.; Koynov, K.; Mohin, J.; Nicolaÿ, R.; Zhang, Y.; Balazs, A. C.; Kowalewski, T.; Matyjaszewski, K. Self-healing polymer films based on thiol−disulfide exchange reactions and self-healing kinetics measured using atomic force microscopy. *Macromolecules* **2012**, *45*, 142−149.
(19) Stukalin, E. B.; Cai, L.-H.; Kumar, N. A.; Leibler, L.; Rubinstein, M. Self-healing of unentangled polymer networks with reversible bonds. *Macromolecules* **2013**, *46*, 7525−7541.
(20) Vlassopoulos, D. Macromolecular topology and rheology: beyond the tube model. *Rheol. Acta* **2016**, *55*, 613−632.
(21) Das, C.; Inkson, N. J.; Read, D. J.; Kelmanson, M. A.; McLeish, T. C. Computational linear rheology of general branch-on-branch polymers. *J. Rheol.* **2006**, *50*, 207−234.
(22) Van Ruymbeke, E.; Bailly, C.; Keunings, R.; Vlassopoulos, D. A general methodology to predict the linear rheology of branched polymers. *Macromolecules* **2006**, *39*, 6248−6259.
(23) Van Ruymbeke, E.; Muliawan, E. B.; Vlassopoulos, D.; Gao, H.; Matyjaszewski, K. Melt rheology of star polymers with large number of small arms, prepared by crosslinking poly (n-butyl acrylate) macromonomers via ATRP. *Eur. Polym. J.* **2011**, *47*, 746−751.
(24) Rubinstein, M.; Semenov, A. N. Dynamics of entangled solutions of associating polymers. *Macromolecules* **2001**, *34*, 1058−1068.
(25) Rubinstein, M.; Dobrynin, A. V. Associations leading to formation of reversible networks and gels. *Curr. Opin. Colloid Interface Sci.* **1999**, *4*, 83−87.
(26) Green, M.; Tobolsky, A. A new approach to the theory of relaxing polymeric media. *J. Chem. Phys.* **1946**, *14*, 80−92.
(27) Chen, Q.; Tudryn, G. J.; Colby, R. H. Ionomer dynamics and the sticky Rouse model. *J. Rheol.* **2013**, *57*, 1441−1462.
(28) Leibler, L.; Rubinstein, M.; Colby, R. H. Dynamics of reversible networks. *Macromolecules* **1991**, *24*, 4701−4707.
(29) Goldansaz, H.; Fustin, C.-A.; Wübbenhorst, M.; van Ruymbeke, E. How Supramolecular Assemblies Control Dynamics of Associative Polymers: Toward a General Picture. *Macromolecules* **2016**, *49*, 1890−1902.
(30) Hawke, L.; Ahmadi, M.; Goldansaz, H.; Van Ruymbeke, E. Viscoelastic properties of linear associating poly (n-butyl acrylate) chains. *J. Rheol.* **2016**, *60*, 297−310.
(31) Ahmadi, M.; Hawke, L. G.; Goldansaz, H.; van Ruymbeke, E. Dynamics of entangled linear supramolecular chains with sticky side groups: Influence of hindered fluctuations. *Macromolecules* **2015**, *48*, 7300−7310.
(32) Scherz, L. F.; Costanzo, S.; Huang, Q.; Schlüter, A. D.; Vlassopoulos, D. Dendronized Polymers with Ureidopyrimidinone Groups: An Efficient Strategy To Tailor Intermolecular Interactions, Rheology, and Fracture. *Macromolecules* **2017**, *50*, 5176−5187.
(33) Stadler, F. J.; Pyckhout-Hintzen, W.; Schumers, J.-M.; Fustin, C.-A.; Gohy, J.-F.; Bailly, C. Linear viscoelastic rheology of moderately entangled telechelic polybutadiene temporary networks. *Macromolecules* **2009**, *42*, 6181−6192.
(34) Van Ruymbeke, E.; Vlassopoulos, D.; Mierzwa, M.; Pakula, T.; Charalabidis, D.; Pitsikalis, M.; Hadjichristidis, N. Rheology and structure of entangled telechelic linear and star polyisoprene melts. *Macromolecules* **2010**, *43*, 4401−4411.
(35) Zhuge, F.; Hawke, L. G.; Fustin, C.-A.; Gohy, J.-F.; Van Ruymbeke, E. Decoding the linear viscoelastic properties of model telechelic metallo-supramolecular polymers. *J. Rheol.* **2017**, *61*, 1245−1262.
(36) Zhang, L.; Chen, L.; Rowan, S. J. Trapping dynamic disulfide bonds in the hard segments of thermoplastic polyurethane elastomers. *Macromol. Chem. Phys.* **2017**, *218*, 1600320.
(37) Imbernon, L.; Oikonomou, E.; Norvez, S.; Leibler, L. Chemically crosslinked yet reprocessable epoxidized natural rubber via thermo-activated disulfide rearrangements. *Polym. Chem.* **2015**, *6*, 4271−4278.
(38) Michal, B. T.; Jaye, C. A.; Spencer, E. J.; Rowan, S. J. Inherently photohealable and thermal shape-memory polydisulfide networks. *ACS Macro Lett.* **2013**, *2*, 694−699.
(39) Kamada, J.; Koynov, K.; Corten, C.; Juhari, A.; Yoon, J. A.; Urban, M. W.; Balazs, A. C.; Matyjaszewski, K. Redox responsive behavior of thiol/disulfide-functionalized star polymers synthesized via atom transfer radical polymerization. *Macromolecules* **2010**, *43*, 4133−4139.
(40) Sprakel, J.; Spruijt, E.; van der Gucht, J.; Padding, J.; Briels, W. Failure-mode transition in transient polymer networks with particle-based simulations. *Soft Matter* **2009**, *5*, 4748−4756.
(41) Capone, B.; Coluzza, I.; LoVerso, F.; Likos, C. N.; Blaak, R. Telechelic star polymers as self-assembling units from the molecular to the macroscopic scale. *Phys. Rev. Lett.* **2012**, *109*, 238301.
(42) Wadgaonkar, I.; Chatterji, A. Network formation and gelation in telechelic star polymers. *J. Chem. Phys.* **2017**, *146*, 084906.
(43) Kryven, I.; Iedema, P. Transition into the gel regime for free radical crosslinking polymerisation in a batch reactor. *Polymer* **2014**, *55*, 3475−3489.
(44) Doi, M.; Edwards, S. F. *The Theory of Polymer Dynamics*; Oxford University Press: 1988; Vol. 73.
(45) Rubinstein, M.; Colby, R. H. *Polymer Physics (Chemistry)*; Oxford University Press: 2003.
(46) Panja, D.; Barkema, G. T.; van Leeuwen, J. Efficient simulation of semiflexible polymers. *Phys. Rev. E* **2015**, *92*, 032603.
(47) Barkema, G. T.; Van Leeuwen, J. A model for the dynamics of extensible semiflexible polymers. *J. Stat. Mech.: Theory Exp.* **2012**, *2012*, P12019.
(48) Barkema, G. T.; Panja, D.; Van Leeuwen, J. Semiflexible polymer dynamics with a bead-spring model. *J. Stat. Mech.: Theory Exp.* **2014**, *2014*, P11008.
(49) Khatri, B. S.; McLeish, T. C. Rouse model with internal friction: A coarse grained framework for single biopolymer dynamics. *Macromolecules* **2007**, *40*, 6770−6777.
(50) Toshchevikov, V.; Gotlib, Y. Y. Relaxation spectrum of a polymer network with included particles: A regular cubic network model with mutual friction. *Polym. Sci., Ser. A* **2013**, *55*, 556−569.
(51) Toshchevikov, V. P.; Gotlib, Y. Y. Shear dynamic modulus of nematic elastomers: modified Rouse model. *Macromolecules* **2009**, *42*, 3417−3429.
(52) Brodeck, M.; Alvarez, F.; Moreno, A. J.; Colmenero, J.; Richter, D. Chain Motion in Nonentangled Dynamically Asymmetric Polymer Blends: Comparison between Atomistic Simulations of PEO/PMMA and a Generic Bead- Spring Model. *Macromolecules* **2010**, *43*, 3036−3051.
(53) Niedzwiedz, K.; Wischnewski, A.; Monkenbusch, M.; Richter, D.; Genix, A.-C.; Arbe, A.; Colmenero, J.; Strauch, M.; Straube, E. Polymer chain dynamics in a random environment: heterogeneous mobilities. *Phys. Rev. Lett.* **2007**, *98*, 168301.

DOI: 10.1021/acs.macromol.7b02613
Macromolecules 2018, 51, 2872−2886

(54) Niedzwiedz, K. *Polymer Dynamics in Miscible Polymeric Blends*; University of Munster: 2007.
(55) Likos, C.; Löwen, H.; Watzlawek, M.; Abbas, B.; Jucknischke, O.; Allgaier, J.; Richter, D. Star polymers viewed as ultrasoft colloidal particles. *Phys. Rev. Lett.* **1998**, *80*, 4450.
(56) Vlassopoulos, D.; Fytas, G.; Pakula, T.; Roovers, J. Multiarm star polymers dynamics. *J. Phys.: Condens. Matter* **2001**, *13*, R855.
(57) Liu, L.; Padding, J.; den Otter, W. K.; Briels, W. J. Coarse-grained simulations of moderately entangled star polyethylene melts. *J. Chem. Phys.* **2013**, *138*, 244912.
(58) Zimm, B. H.; Kilb, R. W. Dynamics of branched polymer molecules in dilute solution. *J. Polym. Sci.* **1959**, *37*, 19−42.
(59) Padding, J.; Briels, W. J. Uncrossability constraints in mesoscopic polymer melt simulations: non-Rouse behavior of C 120 H 242. *J. Chem. Phys.* **2001**, *115*, 2846−2859.
(60) Padding, J.; Briels, W. J. Time and length scales of polymer melts studied by coarse-grained molecular dynamics simulations. *J. Chem. Phys.* **2002**, *117*, 925−943.
(61) Pahnke, K.; Brandt, J.; Gryn'ova, G.; Lindner, P.; Schweins, R.; Schmidt, F. G.; Lederer, A.; Coote, M. L.; Barner-Kowollik, C. Entropy driven chain effects on ligation chemistry. *Chem. Sci.* **2015**, *6*, 1061−1074.
(62) Schwarzl, F. On the interconversion between viscoelastic material functions. *Pure Appl. Chem.* **1970**, *23*, 219−234.
(63) Emri, I.; Von Bernstorff, B.; Cvelbar, R.; Nikonov, A. Re-examination of the approximate methods for interconversion between frequency-and time-dependent material functions. *J. Non-Newtonian Fluid Mech.* **2005**, *129*, 75−84.
(64) Hansen, J.-P.; Verlet, L. Phase transitions of the Lennard-Jones system. *Phys. Rev.* **1969**, *184*, 151.
(65) McLeish, T. Tube theory of entangled polymer dynamics. *Adv. Phys.* **2002**, *51*, 1379−1527.
(66) Fetters, L. J.; Kiss, A. D.; Pearson, D. S.; Quack, G. F.; Vitus, F. J. Rheological behavior of star-shaped polymers. *Macromolecules* **1993**, *26*, 647−654.
(67) Kapnistos, M.; Semenov, A. N.; Vlassopoulos, D.; Roovers, J. Viscoelastic response of hyperstar polymers in the linear regime. *J. Chem. Phys.* **1999**, *111*, 1753−1759.
(68) Xiao-Hong, L.; Xiao-Yang, G.; Xian-Zhou, Z. Structural properties and S−S dissociation energies in a series of disulfide compounds: a theoretical study. *J. Sulfur Chem.* **2011**, *32*, 419−426.
(69) Koval', I. V. The chemistry of disulfides. *Russ. Chem. Rev.* **1994**, *63*, 735−750.
(70) Stans, M. *Bond Dissociation Energies in Simple Molecules*; NIST Library of Congress: 1970.

DOI: 10.1021/acs.macromol.7b02613
Macromolecules 2018, 51, 2872−2886